Check for updates

Experimental and Numerical Evaluation of Thermal Performance of Parabolic Solar Collector Using Water/Al$_2$O$_3$ Nano-fluid: A Case Study

Shahin Nayerdinzadeh[1] · Milad Babadi Soultanzadeh[1] · Mojtaba Haratian[1] · Ashkan Zamanimehr[1]

Abstract

Energy demand keeps growing all over the world and is contributing to climate change. So, fossil fuels must be replaced by renewable energies. Solar energy is the most accessible energy in Iran as well as in many other countries. Parabolic solar collectors appear to be a very promising technology in solar energy absorption. Meanwhile, nano-fluids are known to improve the heat transfer capabilities in comparison with ordinary pure fluids. In this work, an experimental study was applied to solar collectors using water/Al$_2$O$_3$ nano-fluid located in a renewable energy site of Islamic Azad university of Khomenishahr branch followed by numerical simulations. Experimental tests were conducted for 2, 3, and 4 L·min^{-1} flow rates with pure water and 0.1 %, 0.2 %, and 0.3 % volume fraction of nanoparticles, respectively, with the results validating the numerical simulations. The results revealed that reductions in flow rate and elevations in volume fraction led to increased outlet temperature of solar collector, inlet and outlet temperature difference in collector, tank and radiator, and improved solar collector efficiency. Also, heat transfer coefficient rose with augmenting the flow rate and volume fraction.

List of Symbols

A Surface area (m^2)
Q Heat transfer (J)
D Diameter (m)
I Incidence solar flux (w·m^{-2})
Re Reynolds number

✉ Milad Babadi Soultanzadeh
milad.babadi@iaukhsh.ac.ir

[1] Mechanical Engineering Department, Khomeinishahr Branch, Islamic Azad University, Isfahan 8418148499, Iran

S_m Energy generation (w·m^{-3})
U Velocity vector
T Temperature (°C)
f Friction factor
g Gravity (m·s^{-2})
h Heat transfer coefficient (w·m^{-2}·k^{-1})
n Refraction coefficient
P Pressure (Pa)
Pr Prandtl number
c_p Specific heat (J·kg^{-1}·k^{-1})
r Position vector
s Path duration
$\vec{s}$ Direction vector
s' Distribution direction vector
u_y Velocity component y direction (m·s^{-1})
u_x Velocity component x direction (m·s^{-1})
t Time (s)
in Inlet parameters
out Outlet parameters
np Nanoparticle
bf Base fluid
$Q^{,}$ State function
τ Stress tensor
α Absorption coefficient
σ Stefan–Boltzmann constant $5.670\,367 \times 10^{-8}$ (kg·s^{-3}·k^{-4})
σ_s Scattering coefficient
ρ Density (kg·m^{-3})
η Collector efficiency
Ω Solid angle
μ Dynamic viscosity (kg·m^{-1}·s^{-1})

1 Introduction

Since 1970s, due to the increase in global energy demand and cost of fossil fuels, greater attention has been paid to the use of renewable energy resources. Utilization of renewable energy can lead to reduction of greenhouse gas effects. [1]. Irregular utilization of fossil fuels has placed Iran among the top 20 countries in terms of greenhouse gas emissions. Meanwhile, solar energy is the most abundant renewable energy source in the world. The average solar radiation in Iran is about 1800 to 2200 kWh·m^{-2} per year, which is higher than the global standard [2]. Solar energy can be converted to thermal energy using solar collectors. Solar energy can potentially be used for low-temperature industrial processes and domestic water heating. One of the most hopeful technologies to harness the energy of solar radiation is parabolic trough collectors [3]. Thermal performance of parabolic trough collectors can be improved by amplifying the thermal conductivity of the operating fluid. Generally,

thermal conductivity of metals and metal oxide particles are higher than that of liquids. Addition of these particles in nanoscale to operating fluids leads to enhanced thermal conductivity of the heat transfer fluid.

In recent years, many studies have been conducted on the effect of nanoparticles on the thermal performance of solar collectors. Tyagi et al. [4], in a numerical study, investigated the effect of Al_2O_3/water nano-fluids on the thermal performance of direct absorption solar collectors. They used nanoparticles with 20 nm diameter and volume fraction between 0.1 % and 5 % water. They revealed that increase in nanoparticle concentration led to enhanced thermal efficiency by about 10 %. He et al. [5] conducted an experimental study on the thermal performance of the direct absorption of solar collector using water/CuO nano-fluid as operating fluid and adding surfactant. Their results suggested that by increasing the size of the nanoparticles and volume fraction of the nano-fluid, the heat transfer diminished. Karami et al. [6], in an experimental study, investigated the effect of CuO nanoparticles on the thermal efficiency of direct absorption solar collectors. Their experimental results revealed that adding nanoparticles to the base fluid led to augmented thermal efficiency. In another experimental study, Yousefi et al. [7] investigated the effect of nano-fluid Al_2O_3/water on improving the thermal performance of flat-plate solar collectors. They found that the efficiency for nano-fluid 0.2 %wt was 28 % greater than for the based fluid. Qinbo et al. [8] performed an experimental study on the efficiency of flat-plate solar collectors in the presence of nano-fluids as working fluid. They used nanoscale Cu particles in different sizes and volume fractions. Their results indicated that the collector's efficiency with nano-fluid was greater in comparison to the case when the base fluid was used as working fluid. Other results of their experiment included the higher storage temperature of the reservoir when used as nano-fluid. Nang et al. [9] theoretically evaluated the efficiency of flat-plate solar collectors with CuO/water nanoparticles as operating fluid for domestic utilization in the country of Myanmar. They measured the effect of nanoparticle size and the volumetric percentages of nanoparticles. Their results demonstrated that particle size variations had a small effect on the collector efficiency, but increasing the amount of nanoparticles would raise the efficiency. Ghaderian et al. [10] studied the effect of nano-fluid/Al_2O_3 on the thermal efficiency of vacuum tube solar collectors. The diameter of nanoparticles was 40 nm with volume fractions 0.03 % and 0.06 %. It was conducted as a laboratory cycle which a volume flow rate which grew from 20 L to 60 L per hour. Their results revealed that the highest yield was related to nano-fluids with 60 $L·h^{-1}$ and volume fraction 0.06. Ghasemi and Ranjbar [11] in a numerical study investigated the effect of nanoparticles volume fraction on the thermal performance of parabolic solar collectors. They found that the nano-fluid increased the heat transfer in comparison with the base fluid. They also observed that elevation of the volume fraction of nano-fluid enhanced the heat transfer characteristics. Mwesigye and Hwan [12] concluded that the thermal and thermodynamic performance of parabolic trough collectors with Syltherm800/AL_2O_3 nano-fluid improved in comparison with the case of using base fluid. Coccia et al. [3] in a numerical analysis evaluated the annual performance of a low-temperature parabolic trough collector. They used

six nano-fluids at different volume fractions to improve the thermal performance of this system. Kasayian et al. [13] examined parabolic solar collectors for a laboratory sample to illustrate ways of amplifying the efficiency of this collector. They managed to build a collector with a width of 0.7 and length of 2 m with steel mirrors. In order to reach the best collector type, they used four types of absorbent tubes. They tested them using nano-fluid carbon/oil nanotubes with a volumetric volume of 0.2 and 0.3 as the operating fluid. They found that the absorbent copper tube covered with chromium had the highest absorption and thermal conductivity, where the overall collector efficiency increased for 0.2 %, 0.3 %, 5 % and 7 % for the nano-fluid. Zadeh et al. [14] focused on improving the efficiency and optimization of the parabolic solar collector in a numerical study. They considered the thermal fluxes of the absorbent tube as non-uniform, and used Al_2O_3 synthetic oil nano-fluid. Their results indicated that elevation of the heat transfer had a direct relationship with the nanoparticle volume fraction and inverse relationship with the operational collector temperature. Wang et al. [15] examined the effect of nano-fluid in parabolic solar collectors in a numerical study. They used synthetic oil as a base fluid and used Al_2O_3 nano-particles. They found that use of nano-silver reduced the temperature gradient and increased the efficiency of the collector. Menbari et al. [16] conducted an experimental and analytical study of the effect of CuO/water nano-fluid on the efficiency of a direct absorption parabolic solar collector. Their results suggested that the thermal performance of collector improved using the nano-fluid.

In this paper, a parabolic solar collector installed in Islamic Azad University, Khomeini Shahr branch renewable energies site is studied experimentally and numerically in order to examine effect of nanoparticle addition to the base fluid on the thermal performance of parabolic trough collectors.

2 Experimental Setup

2.1 Collector Details

A solar parabolic collector includes a parabolic reflector and absorber tube, installed on the focal distance of parabolic reflector. The parabolic solar collector utilized in this work had 4.1 m length and an aperture width of 2 m. The parabolic reflection was made of thin steel mirror sheets. For making the reflector, a body structure was made by steel after which parabolic sheets were placed on the body. Figure 1 demonstrates the parabolic trough collector studied in this research. Also, Table 1 reveals the dimensions of the parabolic reflector.

Absorber tube is the most important and complicated part for parabolic collectors. In this system, an absorber tube was used made of copper tube with black chrome coating which was attached to a glass pipe composed of quart glass for high transmission. The space between the absorber tube and glass envelope was vacuumed. This vacuumed space caused elevation of the heat transfer and avoided convection heat losses.

Fig. 1 Photo of parabolic trough collector

**Table 1** Apparent characteristic of pilot

Specifications	Descriptions and details
Collector length	4.1 m
Aperture width	2 m
Absorbent tube length	4.1 m
The inner diameter of the absorbent tube	36 mm
The outer diameter of absorbent tube	38 mm
Inner diameter of the glass envelope	56 mm
Outer diameter of the glass envelope	60 mm
Transmittance of glass envelope	0.9
Absorber absorption coefficient	0.95
Geometrical concentration factor	18.18
Actual concentration factor	6.225
Intercept factor	0.713

2.2 Nano-fluid Preparation

In this study, Al_2O_3 powder was employed with a size of 20 nm, where the nano-fluid was made by a two-step method. The nanoparticles were created into dry powders and mixed in the base fluid by ultrasonic instigator (Hielscher UP-200S ultra
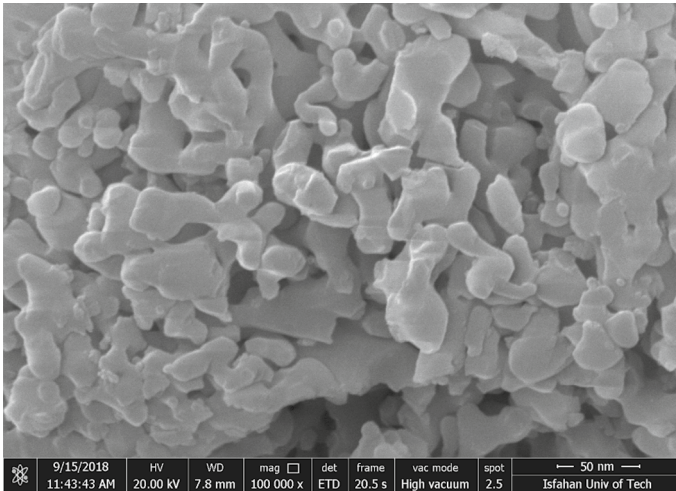
Fig. 2 FESEM micrographs of Al_2O_3 nanoparticles
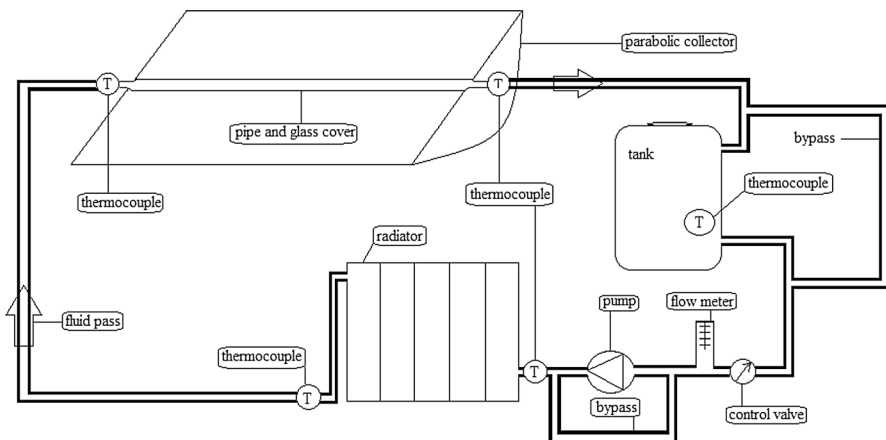
Fig. 3 The experimental setup of the hydraulic cycle

sonic model). A scanning electron microscope FESEM (field emission scanning electron microscope) was employed to estimate the nano-powder size (Fig. 2).

2.3 Hydraulic Cycle and Data Collection Procedure

The cycle employed to evaluate the thermal performance of parabolic solar collector in this work is demonstrated in Fig. 3. In this prototype, Al_2O_3/water was used as the operating fluid. To measure the solar direct irradiance, a solar power meter (1333R) was utilized. Further, the inlet and outlet temperature of collectors as well as the inlet and outlet temperature of radiator and tank temperature were measured

by K type thermocouples and monitored by data logger (TES-1384). In this study, the flow rate was controlled by a flow meter within the range of 10–100 L H^{-1}.

3 Numerical Method

3.1 Governing Equations

In order to compare the simulation results and experimental data, the determined parabolic solar collector was simulated. This simulation was conducted in 2 parts. In the first part, non-uniform heat flux distribution on the outer wall of the absorber tube was obtained by DO (discrete orientation) radiation model. The DO radiation model equation is presented in Eq. 1 [17]. In the second part, the thermal characteristics of the operating fluid were then calculated.

$$\nabla \cdot \left(I(\vec{r} \cdot \vec{s})\vec{s} \right) + \left(a + \sigma_s \right) I(\vec{r} \cdot \vec{s}) = an^2 \frac{\sigma T^4}{4\pi} + \frac{\sigma_s}{4\pi} \int_0^{4\pi} I(\vec{s} \cdot \vec{s'})\varphi'\left(\vec{s} \cdot \vec{s'} \right) d\Omega \quad (1)$$

In this study, the fluid flow was turbulent and in a steady-state condition. So, the governing equations for continuity, momentum, energy, as well as standard k and ε two equation turbulence model can be written as follows [18]:

Continuity equation:

$$\frac{\partial}{\partial u_i}(\rho u_i) = 0. \quad (2)$$

Momentum equation:

$$\frac{\partial}{\partial x_i}\left(\rho u_i u_j \right) = -\frac{\partial P}{\partial x_i} + \frac{\partial}{\partial x_i}\left[(\mu_t + \mu)\left(\frac{\partial u_i}{\partial x_j} + \frac{\partial u_j}{\partial x_i} \right) - \frac{2}{3}(\mu_t + \mu)\frac{\partial u_l}{\partial x_l}\delta_{ij} \right] + \rho g_i. \quad (3)$$

Energy equation:

$$\frac{\partial}{\partial x_i}(\rho u_i T) = \frac{\partial}{\partial x_i}\left[\left(\frac{\mu}{Pr} + \frac{\mu_t}{\sigma_T} \right) \frac{\partial T}{\partial x_i} \right] + S_R. \quad (4)$$

k equation:

$$\frac{\partial}{\partial x_i}(\rho u_i k) = \frac{\partial}{\partial x_i}\left[\left(\mu + \frac{\mu_t}{\sigma_k} \right) \frac{\partial k}{\partial x_i} \right] + G_k - \rho\varepsilon. \quad (5)$$

ε equation:

$$\frac{\partial}{\partial x_i}(\rho u_i \varepsilon) = \frac{\partial}{\partial x_i}\left[\left(\mu + \frac{\mu_t}{\sigma_\varepsilon} \right) \frac{\partial \varepsilon}{\partial x_i} \right] + \frac{\varepsilon_k}{k}(C_1 G_k - C_2 \rho\varepsilon), \quad (6)$$

where μ_t and G_k represent the turbulent viscosity and production rate of k, respectively:

$$G_k = \mu_t \frac{\partial u_i}{\partial x_j}\left(\frac{\partial u_i}{\partial x_j} + \frac{\partial u_j}{\partial x_i}\right) \cdot \mu_t = C_\mu \rho \frac{k^2}{\varepsilon}. \tag{7}$$

The standard constants used were as follows: $C_\mu = 0.09, C_1 = 1.44, C_2 = 1.92, \sigma_k = 1, \sigma_\varepsilon = 1.3, \sigma_T = 0.85$.

The thermal efficiency of the parabolic solar collector is defined as follows [16]:

$$\eta = \frac{\dot{m}\, C_p (T_{out} - T_{in})}{AI}, \tag{8}$$

where A and I represent the aperture area and incidence solar flux, respectively.

3.2 Thermo-physical Properties of the Nano-fluid

Utilization of nano-fluids in the base fluid improves the characteristics of the operating fluid. The nano-fluid properties depend on temperature and volume fraction of nano-fluids. The density of the nano-fluid is represented by Eq. 9—[19]:

$$\rho_{nf} = \rho_{bf}(1 - \varphi) + \rho_{np}\varphi. \tag{9}$$

The specific heat capacity of the nano-fluid is given by Eq. 10:

$$C_{pnf} = \frac{\rho_{nf}(1 - \varphi)C_{pbf}}{\rho_{nf}} + \frac{\rho_{np}\varphi C_{pnp}}{\rho_{nf}}. \tag{10}$$

For calculating the thermal conductivity, Eq. 11 is presented:

$$K_{nf} = \frac{K_{np} + 2K_{bf} + 2\varphi(K_{np} - K_b)}{K_{np} + 2K_{bf} - \varphi(K_{np} - K_b)}. \tag{11}$$

The nano-fluid viscosity is calculated as the next equation:

$$\mu_{nf} = \mu_{bf}(1 + (2/5\varphi) + 6/5\varphi^2). \tag{12}$$

In these equations, φ, bf, and np represent volume fraction, base fluid, and nano-particle, respectively. As displayed in Fig. 4, the geometry and mesh grid created using software GAMBIT and governing equations are solved using finite volume method via CFD (computational fluid dynamics) commercial software Fluent 16.0.

3.3 Boundary Conditions

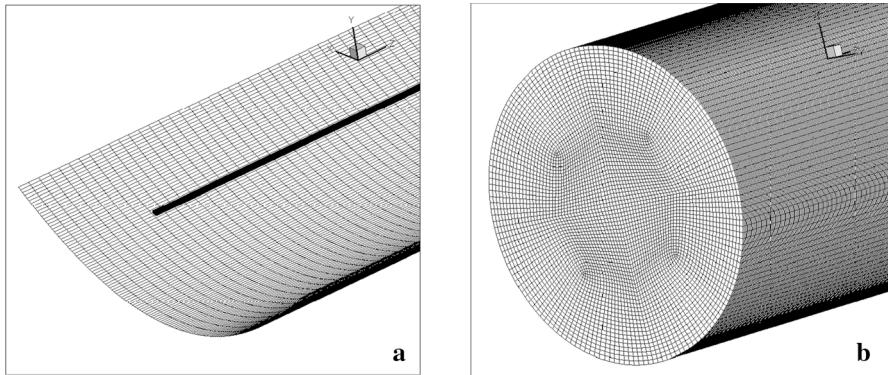The following boundary conditions are used for simulation of the absorber tube.

Inlet boundary conditions:

The operating flow has a uniform velocity at the absorber inlet.

$$U = u_{in},\ T = T_{in}\ at\ L = 0.$$

Wall boundary condition:

Fig. 4 Generated mesh (a) reflector (b) absorber tube

For inside of the absorber tube, non-slip condition is considered. The top of the absorber tube received a uniform heat flux, while its bottom received a distributed heat flux as revealed in Fig. 5.

Outlet boundary condition:

Outflow boundary condition is considered for the outlet of absorber tube at $L = 4.1$ m.

To obtain the best mesh size, grid independent test was conducted for two steps of simulation. The first part of simulation was performed for four grids where heat flux distribution was estimated for all four grids. Finally, the grid with 686 000 mesh cells was found suitable for the first part of simulation. To find the best size of mesh

wall-fluxe: 4600 5200 5800 6400 7000 7600
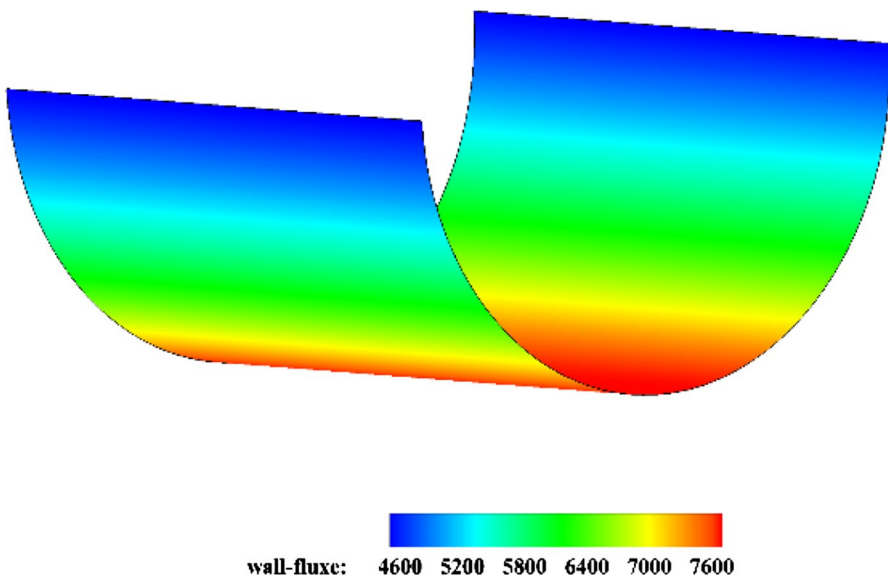
Fig. 5 Heat flux distribution on the absorber tube ($w \cdot m^{-2}$)

for the second part of simulation, as with the first part, this test was conducted for four grids with the outlet temperature evaluated. The grid with 1 121 845 mesh cells proved to be suitable for the second part.

4 Results and Discussion

The experiments were conducted in July and August 2017 in Esfahan, Iran (latitude 32.6933˚, 51.5360˚). In these experiments, effect of three volume fractions 0.1 %, 0.2 %, and 0.3 % Al_2O_3/water nano-fluid and volume flow rate 2, 3, 4 $L \cdot min^{-1}$ was analyzed and the results were compared with water as operating fluid. The experiments were conducted on a daily basis between 11:30 a.m. and 12:30 p.m. during summer. The simulations were done in two sections: the first section was carried out to obtain the distribution of heat flux on the absorber tube; and in second part the parameters of operating fluid were obtained using the results of the first section.

4.1 Experimental Results

Solar radiation heat flux is measured for four different days and is indicated in Fig. 6. All measurements conducted using TES-1333R solar meter with 0.1 W m^{-2} resolution which has been installed on collector axis that rotate by a sun tracker. Regarding the figure, solar radiation increased from 11:30 to 12:15 and after that it had a constant behavior until 12:30.
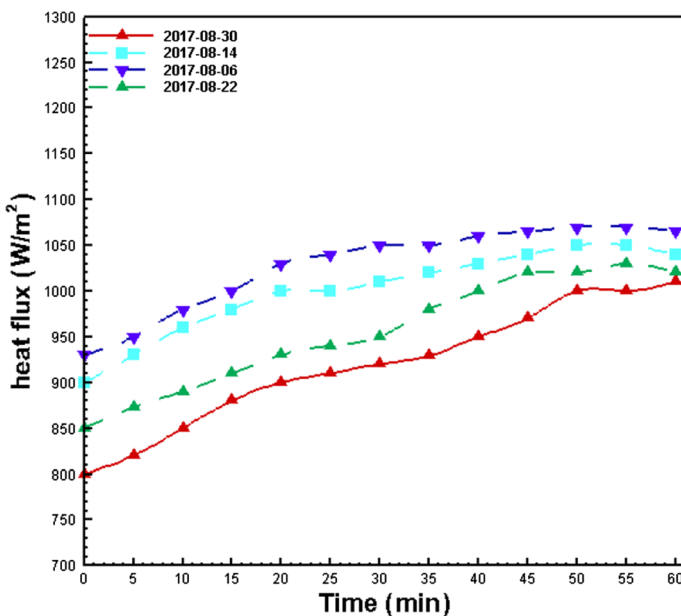

Fig. 6 Measured solar heat flux in four different days

The results of the inlet, outlet, and ambient temperatures of the operating fluid are indicated in Fig. 7a–d. It clearly shows that over time the temperature increased, and then constant temperatures were achieved. The figure also reveals that increasing the volume fraction of nano-fluid and reducing the volume flow rate of the operating fluid enhanced the inlet and outlet temperatures.

Figure 8a–c displays the experimental results of outlet temperature of parabolic solar collectors for volume flow rate 2, 3 and 4 L·min^{-1}. It is clear from Fig. 8 that there is initial rise in outlet temperatures over time, after which the temperatures become constant. This figure demonstrated that the system has been stated steady.

Figure 9a–c indicates inlet and outlet temperature difference for 2,3 and 4 L·min^{-1}. This figure indicates an initial growth in temperature difference over time after which the temperature difference becomes constant. Indeed, after about 1 h, the system became stable. It is clear from Fig. 9 that elevation of the volume fraction of nano-fluid caused augmented temperature difference.

The tank temperature has been reported using tank's thermocouple. Figure 10a–c displays that at lower volume flow rates, the tank temperature increased. Also
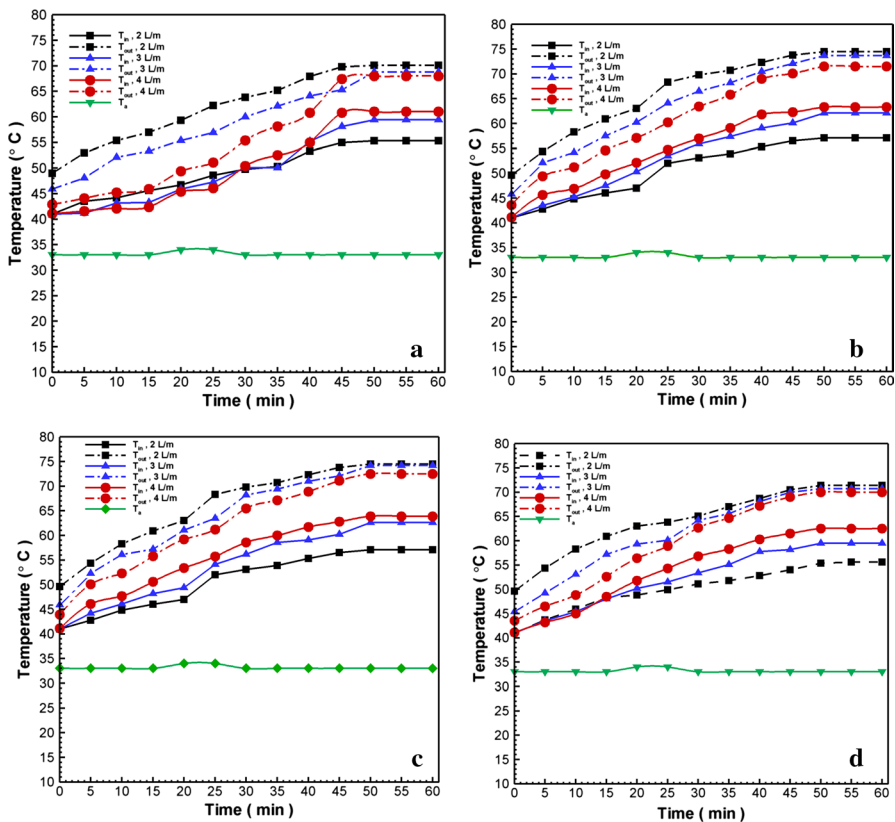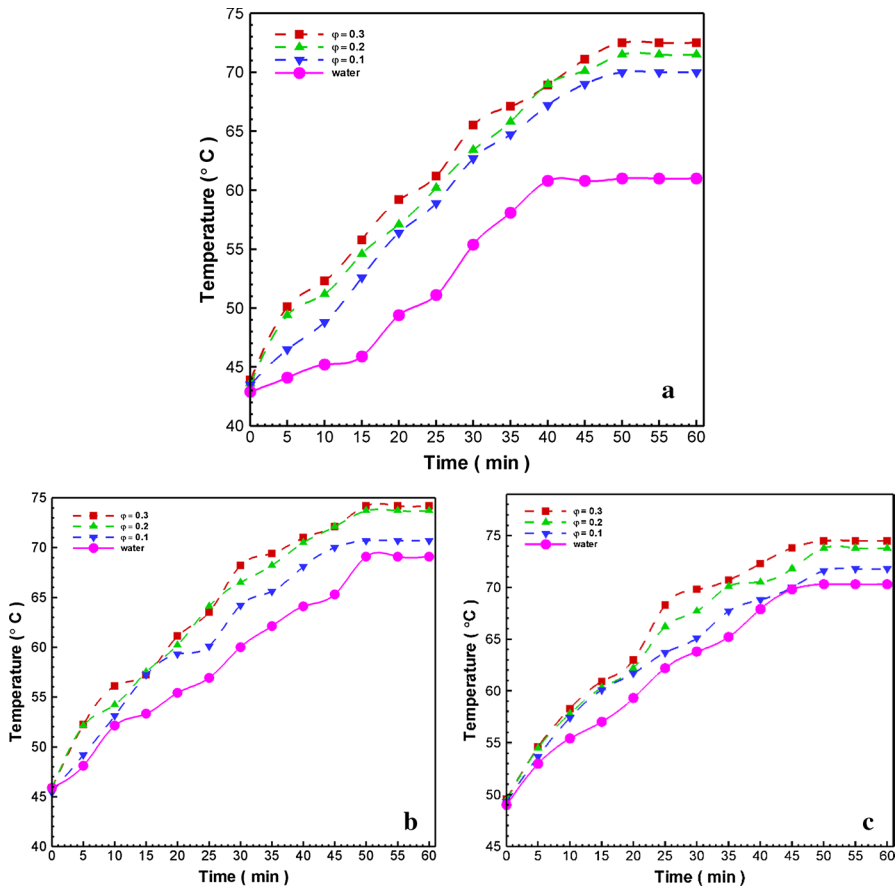

Fig. 7 Inlet and outlet temperature in parabolic collectors for (a) water, (b) nano-fluid 0.1 %, (c) nano-fluid 0.2 %, (d) nano-fluid 0.3 %

Fig. 8 Outlet temperature for volume flow rates (a) 2, (b) 3 and (c) 4 L·min^{-1}

elevation of the volume fraction of nano-fluid increased the tank temperature, as in the circulation flow rate, thermal conductivity affects the tank temperature.

Figure 11 illustrates radiator inlet temperature differences at 1 h time period for various volume fractions at 2, 3 and 4 L·min^{-1} flow rates, respectively. According to Fig. 11, elevation of volume fraction leads to increased radiator inlet temperature across all flow rates along the temperature profile. It reveals that time average radiator inlet temperature rises due to the growth in the volume fraction. Conversely, increase in the flow rate leads to diminished radiator inlet temperature. This happened because of increase in heat transfer rate from absorber tube to operating fluid, indicating the heat transfer increment due to the rise in volume fraction.

Figure 12 illustrates the difference between radiator inlet and outlet temperature for 1 h time period for various volume fractions at 2, 3 and 4 L·min^{-1} flow rates, respectively. Based on Fig. 11, elevation of flow rate leads to diminished radiator inlet and outlet temperature difference while increasing in volume
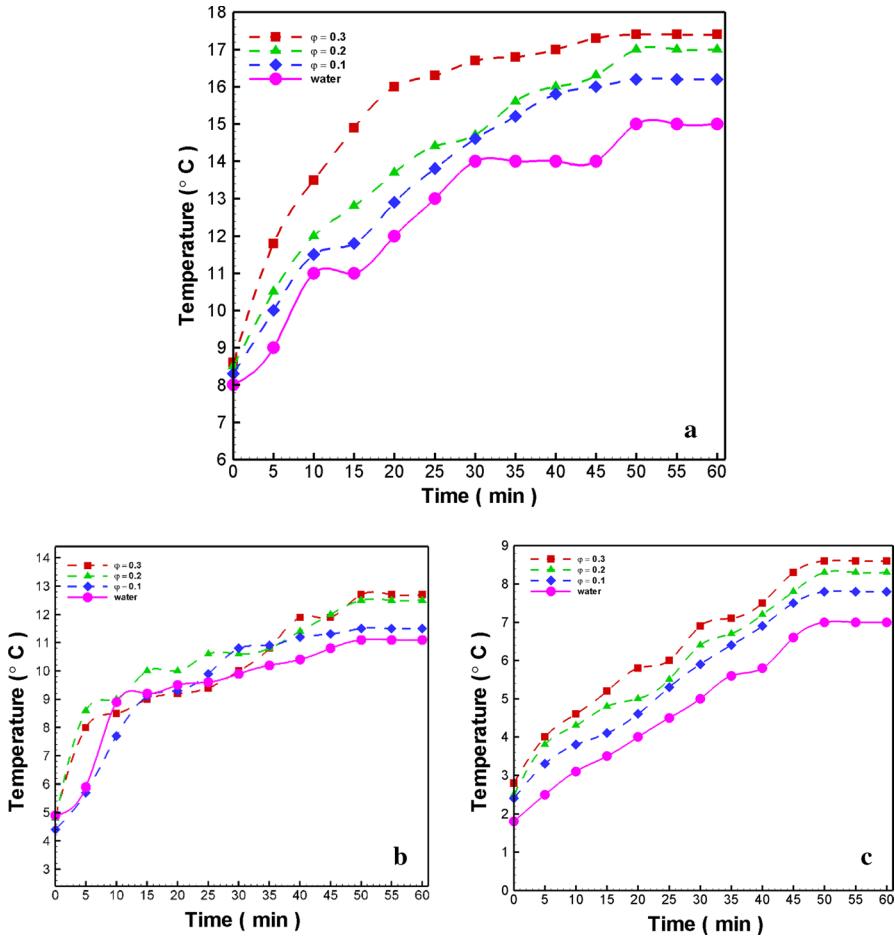
Fig. 9 Temperature difference for volume flow rates (a) 2, (b) 3 and (c) 4 L·min^{-1}

fraction results in enhanced radiator inlet and outlet temperature difference. As the radiator performance is a function of inlet and outlet temperature difference, consequently, an increase in the volume fraction leads to amplified radiator performance. This phenomenon happens because of elevation of convective heat transfer coefficient in the radiator.

Regarding Fig. 13 which illustrates thermal efficiency of studied collector in different inlet temperature when flow rate is 2 L·min^{-1}, thermal efficiency is maximum for all volume fractions when inlet temperature is close to ambient temperature. It means, in constant incidence solar flux, 1.5 centigrade degree increasing in inlet temperature leads to 1.7 % decrease in efficiency. Inlet temperature impact on efficiency has been increased with increasing in nanoparticles concentration.
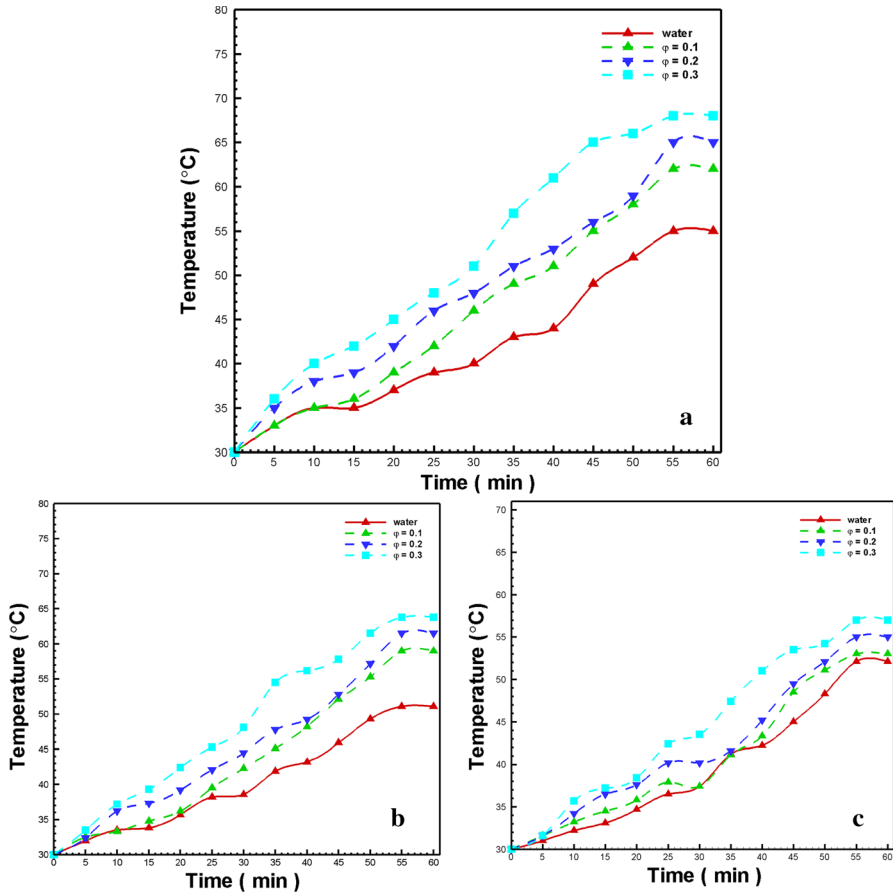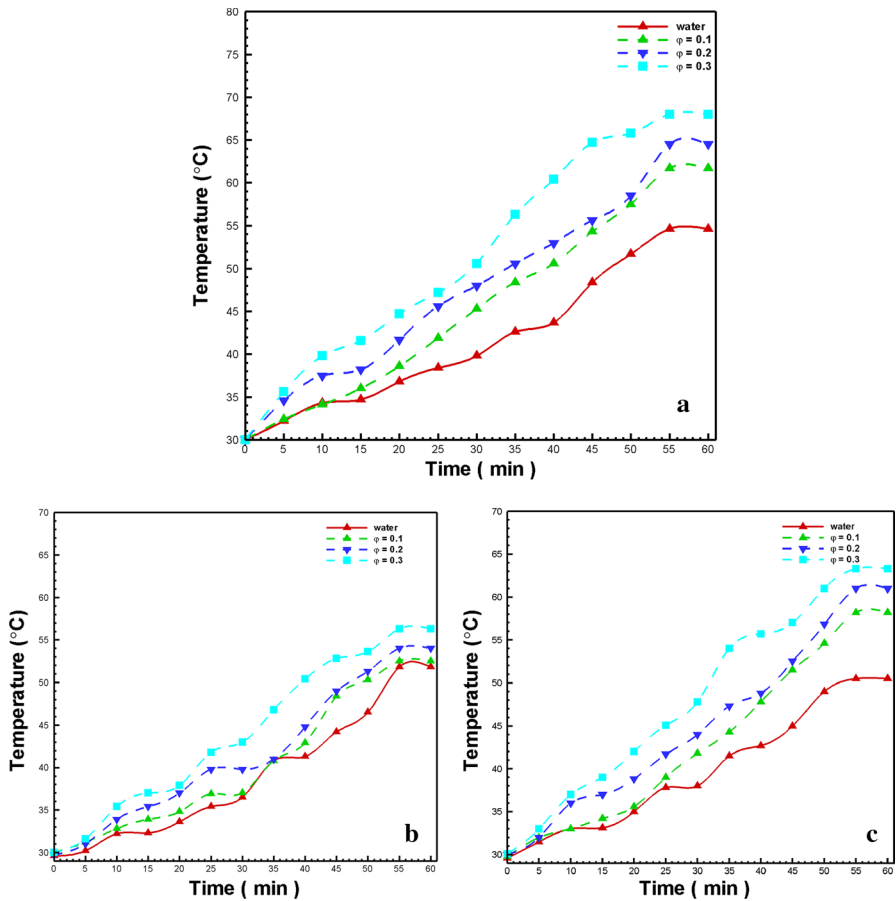
Fig. 10 Tank temperature for volume flow rates (a) 2 (b) 3 and (c) 4 L·min^{-1}

4.2 Numerical Results

In this study, the parabolic trough collector available in Islamic Azad University of Khomeini Shahr is simulated and the effect of nano-fluid on the thermal performance is studied. Finally, numerical results are compared with experimental results. The temperature of the operating flow along the length of the absorber tube for different fluids and volume flow rates is displayed in Fig. 14. The results reveal that increasing the volume fraction of nano-fluid enhanced the thermal conductivity of fluid and improved the heat transfer of the collector. Figure 14 also indicates that reduction of the volume flow rate of the fluid resulted in elevated average temperature.

Figure 15 demonstrates variations in the convection heat transfer coefficient inside the absorber tube for different volume flow rates and volume fractions. It is clear that elevation of the volume flow rate caused enhanced convection heat

Fig. 11 Radiator inlet temperature differences at 1 h time period for volume flow rates (a) 2, (b) 3 and (c) 4 L·min^{-1}

transfer coefficient. Also, the growth of the volume flow rate augmented the heat transfer coefficient.

The effects of volume flow rate and volume fraction of the nano-fluid on the inlet and outlet temperature difference of the fluid and parabolic trough collector's thermal efficiency are indicated in Figs. 16 and 17 both experimentally and numerically. It can be observed in these figures that a good agreement exists between the experimental and numerical results. Figure 15 indicates that reduction of the volume flow rate enhances the inlet and outlet temperature difference of the operating fluid. Figure 16 shows that elevation of the volume flow rate led to diminished thermal efficiency of the parabolic collector. In other words, with the growth of the volume flow rate, the outlet temperature and thermal efficiency declined. Table 2 presents numerical values of deviations between numerical
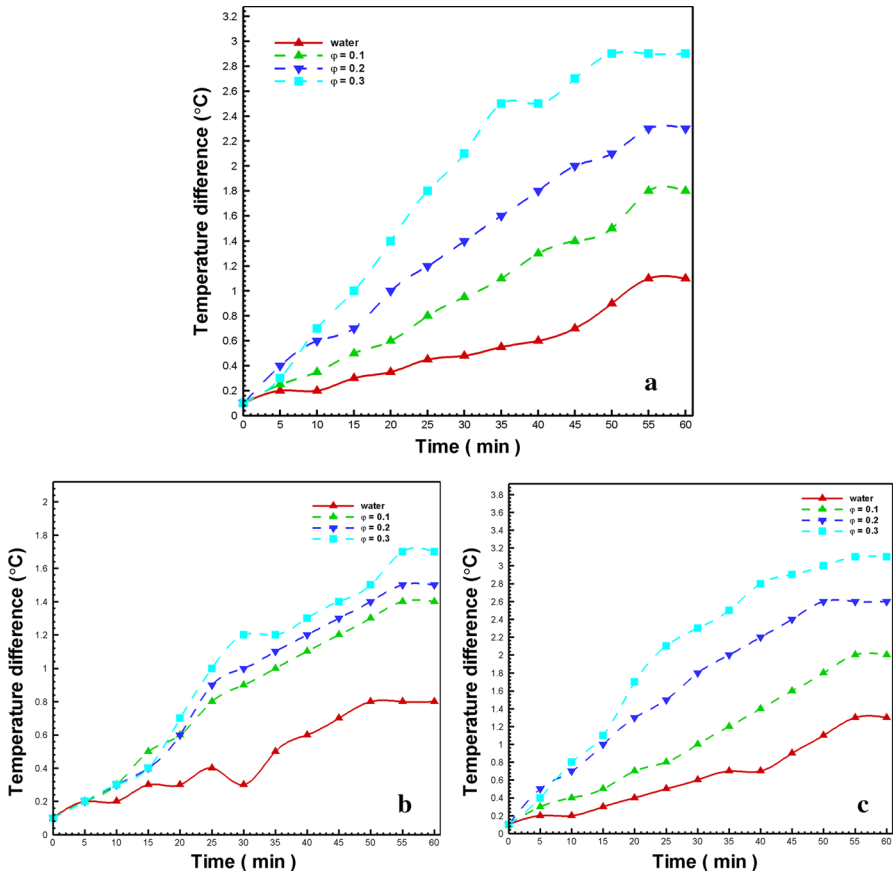
Fig. 12 Difference between radiator inlet and outlet temperatures for 1 h time period for volume flow rates (a) 2, (b) 3 and (c) 4 L·min^{-1}

model and experimental data and Fig. 17 also indicates that the higher nano-fluid concentration has a higher thermal efficiency.
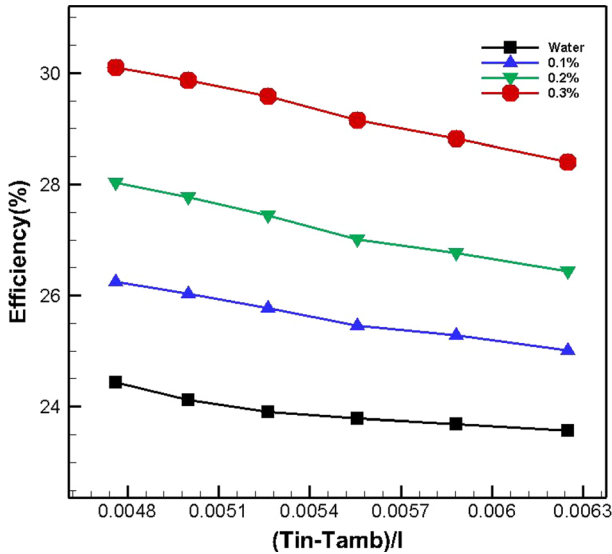
Fig. 13 Thermal efficiency in different $(T_{in} - T_{amb})/I$ for various volume fraction at 2 L·min^{-1} flow rate

5 Conclusion

In this study, the effect of Al_2O_3/water nano-fluid was experimentally and numerically investigated on the thermal performance of parabolic trough collectors. The results indicated that the nano-fluid had a positive effect on the parabolic collector's thermal performance. Numerical results showed that with elevation of the volume fraction of nano-fluids and reduction of the volume flow rate, the outlet temperature rose. Also, the rise the volume fraction amplified the convection heat transfer coefficient. Further, the nano-fluid axial average temperature increased along the length of the absorber tube. Experimental results suggested that enlargement of the volume fraction and reduction of the volume flow rate caused heightened operating fluid's inlet and outlet temperatures, temperature difference of inlet and outlet of fluid, tank's temperature and temperature difference of radiator. The experimental and numerical results indicated that the growth of volume fraction of nano-fluids by elevation of the thermal conductivity of the fluid led to enhanced thermal performance of the collector. Overall, the results suggest that the parabolic collector thermal efficiency was directly contingent upon the nano-fluid concentration; its elevation from 0.1 % to 0.3 % resulted in amplification of thermal efficiency from 26 % to 30.1 % for the volume flow rate 2 L·min^{-1}. Finally, comparison of numerical and experimental results showed their good agreement.
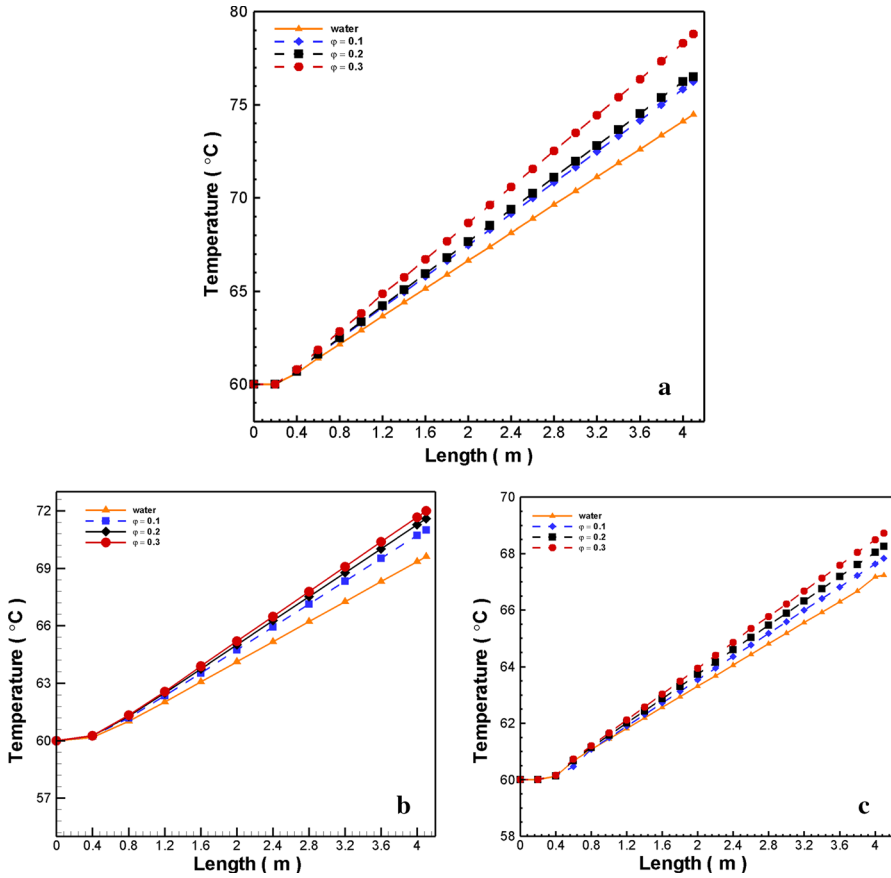
Fig. 14 Temperature of the operating flow along the length of the absorber tube for volume flow rates: (a) 2, (b) 3, and (c) 4 L·min^{-1}
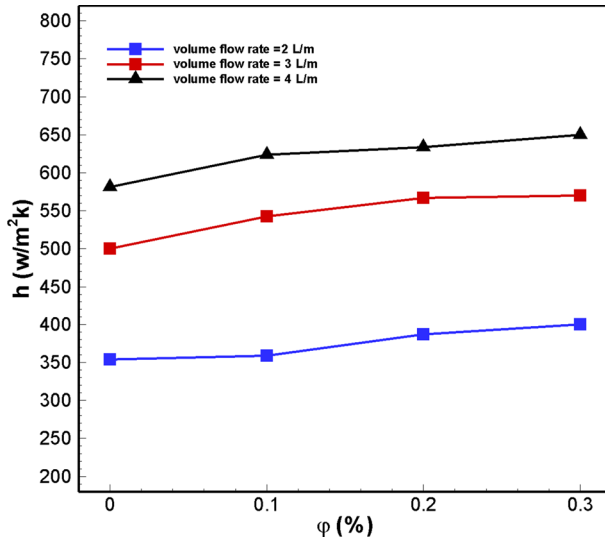
Fig. 15 Variations in the convection heat transfer coefficient inside the absorber tube for different volume flow rates and volume fractions
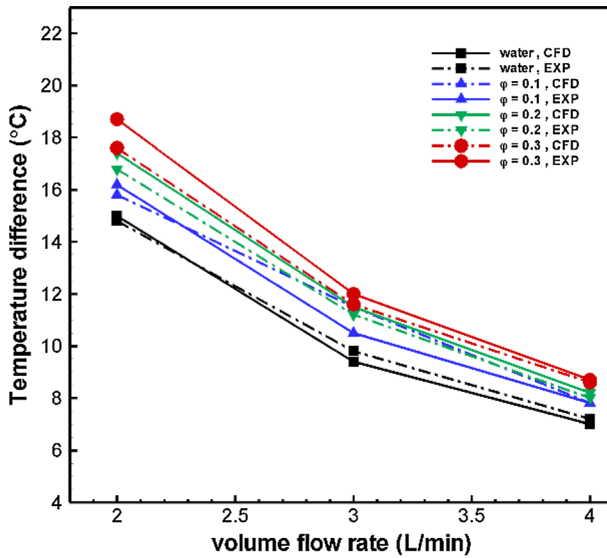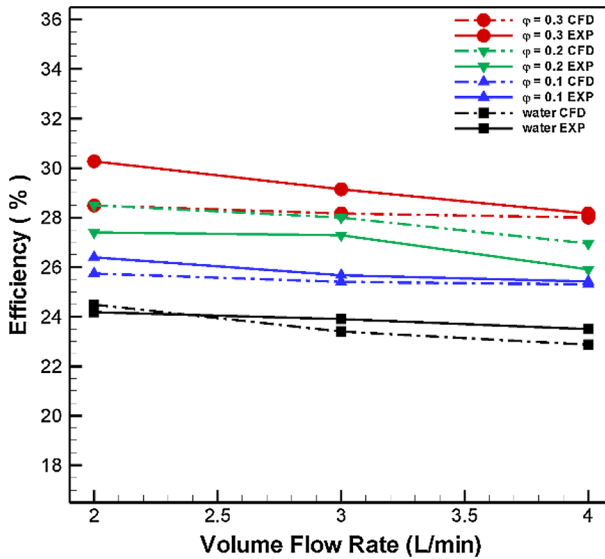

Fig. 16 Effect of volume flow rate and volume fraction of nano-fluid on the inlet and outlet temperature difference

Fig. 17 Effect of volume flow rate and volume fraction of nano-fluid on the parabolic trough collector's thermal efficiency

Table 2 Numerical deviations between numerical model and experimental measurements

	Flow rate (L·min^{-1})		
	2	3	4
Water	0.32	0.5	0.63
$\varphi = 0.1$	0.65	0.26	0.11
$\varphi = 0.2$	1.1	0.72	1.05
$\varphi = 0.3$	1.78	0.98	0.16

References

1. Z. Cheng, Y. He, F. Cu, R.J. Xu, Y.B. Tao, Numerical simulation of a parabolic trough solar collector with nonuniform solar flux conditions by coupling FVM and MCRT method. Sol. Energy **86**, 1770–1784 (2012)
2. P. Alamdari, O. Nematollahi, A. Alemrajabi, Solar energy potentials in Iran: a review. Renew. Sustain. Energy Rev. **21**, 778–788 (2013)
3. G. Coccia, G. Di Nicola, L. Colla, L. Fedele, M. Scattoloni, Adoption of Nano fluids in low-enthalpy parabolic trough solar collectors: numerical simulation of the yearly yield. Energy Convers. Manage. **118**, 306–319 (2016)
4. H. Tyagi, P. Phelan, R. Prasher, Predicted efficiency of a low-temperature Nanofluid-based direct absorption solar collector. J. Sol. Energy Eng. **131**, 4 (2009)
5. Q. He, S. Wang, Z. Zheng, Experimental investigation on photo thermal properties of Nanofluids for direct absorption solar thermal energy systems̀. Energy Convers. Manage. **73**, 150–157 (2013)
6. M. Karami, B. Akhavan, S. Delfani, M. Raisee, Experimental investigation of CuO Nanofluid-based direct absorption solar collector for residential applications. Renew. Sustain. Energy Rev. **52**, 793–801 (2015)

7. T. Yousefi, F. Veysi, E. Shojaeezade, S. Zinadini, An experimental investigation on the effect of Al$_2$O$_3$–H$_2$O Nanofluid on the efficiency of flat-plate solar collectors. Renew. Energy **39**, 293–298 (2012)

8. Q. He, S.H. Zeng, S. Wang, Experimental investigation on the efficiency of flat-plate solar collectors with Nanofluid. Appl. Therm. Eng. **88**, 165–171 (2015)

9. N. Sint, I. Choulhury, H. Masjuki, H. Aoyama, Theoretical analysis to determine the efficiency of a CuO-water Nanofluid based-flat plate solar collector for domestic solar water heating system in Myanmar. Sol. Energy **155**, 608–619 (2017)

10. J. Ghaderian, N. Sidik, An experimental investigation on the effect of Al$_2$O$_3$/distilled water Nanofluid on the energy efficiency of evacuated tube solar collector. Int. J. Heat Mass Transf. **108**, 972–987 (2017)

11. E. Ghasemi, A. Ranjbar, Thermal performance analysis of solar parabolic trough collector using Nanofluid as working fluid: a CFD modeling study. J. Mol. Liq. **222**, 159–166 (2016)

12. A. Mwesigye, Z.H. Meyerd, Thermal and thermodynamic performance of a parabolic trough receiver with Syltherm800-Al$_2$O$_3$Nanofluid as the heat transfer fluid. Energy Procedia **75**, 394–402 (2015)

13. A. Kasaeian, S. Paviran, R. Azarian, A. Rashidi, Performance evaluation and Nanofluid using capability study of a solar parabolic trough collector. Energy Convers. Manage. **89**, 368–375 (2015)

14. P. Zadeh, M.T. Sokhansefat, A. Kasaeian, F. Kovsay, A. Akbarzade, Hybrid optimization algorithm for thermal analysis in a solar parabolic trough collector based on Nanofluid. Energy **82**, 857–864 (2015)

15. Y. Wang, Q. Liu, J. Lei, H. Jin, Performance analysis of a parabolic trough solar collector with non-uniform solar flux conditions. Int. J. Heat Mass Transf. **82**, 236–249 (2015)

16. A. Menbari, A. Alemrajabi, A. Rezaei, Heat transfer analysis and the effect of CuO/Water Nanofluid on direct absorption concentrating solar collector. Appl. Therm. Eng. **104**, 176–183 (2016)

17. Fluent Release 14.0, User's guide, Fluent In C, 2016

18. Z. Cheng, Y. He, J. Xiao, Y. Tao, R. Xu, Three-dimensional numerical study of heat transfer characteristics in the receiver tube of parabolic trough solar collector. Int. Commun. Heat Mass Transfer **37**, 782–787 (2010)

19. E. Bellos, C. Tivanidis, G. Gkinis, Thermal enhancement of solar parabolic trough collectors by using Nanofluids and converging-diverging absorber tube. Renew Energy **94**, 213–222 (2016)